

# CONCURRENT PREDICTIONS OF FLOW, THERMAL AND STRUCTURAL PROPERTIES FOR TEXTILE COMPOSITES

Francois Robitaille

*Department of Mechanical Engineering, University of Ottawa  
161 Colonel By Hall, Ottawa, Ontario, Canada K1N 6N5  
Corresponding author's Email: frobit@genie.uottawa.ca*

**SUMMARY:** This paper presents an application of meso-scale simulations of composite unit cells where in-plane permeability, transverse thermal conductivity and in-plane stiffness are predicted for two reinforcements of varying geometry. The geometry of textile unit cells was modeled with TexGen v2. Meshes featuring up to ~500 000 tetrahedral elements were created using Gambit™ 2.2.30. Flow and heat transfer simulations were performed using Fluent™ 6.2.26 whilst static loading simulations were conducted using Abaqus™ 6.7-1. In-plane permeability, which was strongly affected by tow geometry, was highest for flow along tows in thicker cells. Conductivity was not strongly affected by the cell geometry; thinner cells showed higher values. Contrary to expectations the unidirectional and bi-directional materials behaved similarly. In-plane stiffness values generally followed micromechanical models.

**KEYWORDS:** permeability, conductivity, stiffness, simulation, unit cell

## INTRODUCTION

Meso-scale simulations on textile composite unit cells [1-3] are increasingly used to compare processing and performance properties of reinforcements of different types, and to explore the possibility of predicting these properties reliably and accurately. The aims are to reduce the physical testing needed to determine the properties and to quantify their variability. Efforts presented in the literature have been directed mostly at developing the simulation tools. In this paper an application example is presented where in-plane permeability, transverse thermal conductivity and in-plane stiffness are predicted for two reinforcements of varying geometry. All phenomena are captured and quantified, and some limitations are identified. The effect of reinforcement geometry on these properties is discussed.

## REINFORCEMENT GEOMETRY, DOMAINS AND PARAMETERS

Flow, heat transfer and static loading simulations were conducted on unit cells of  $0^\circ$  and  $0/90^\circ$  non-woven reinforcements. Tow sections were modelled as hyperellipses in their  $x_s, y_s$  local plane, Eqn. 1, Fig. 1. Tows and cells were built in TexGen v2, varying the hyperellipse power  $n$ , ratio  $a_t$  of tow width to tow height  $h_t$ , and ratio of tow height  $h_t$  to cell height. Full-factorial 2-level Taguchi plans 1 and 2 were conducted for materials 1 (runs 1A-1Z,  $0^\circ$ ) and 2 (runs 2A-2Z,  $0/90^\circ$ ). Central points were included for 9 runs per plan and 18 runs in total, Table 1. Fibre mass per unit area was constant at  $\sim 1030 \text{ g/m}^2$  and  $\sim 2060 \text{ g/m}^2$  for materials 1 ( $0^\circ$ ) and 2 ( $0/90^\circ$ ). Tow height and lateral spacing were 1 mm in all simulations. Cell fibre volume fraction  $v_{f,c}$  varied with domain height only. Tow fibre volume fraction  $v_{f,t}$  varied with all other geometric parameters, with values set for theoretical maximum  $v_{f,t} = 0.906$  in tows of smallest section (runs 1G, 1H, 2G, 2H). Meshes built with Gambit™ 2.2.30 featured up to  $\sim 500\,000$  4-noded tetrahedral elements. Faces normal to the  $x, y$  and  $z$  axes were labelled  $x_{min}, x_{max}, y_{min}, y_{max}, z_{min}$  and  $z_{max}$ . Volumes were labelled *tow 1, tow 2, ..., resin*. Tows extended along  $y$  only for material 1 in runs 1A-1Z. Material 2 was balanced along  $x$  and  $y$  axes in runs 2A-2Z, with double cell height.

$$y_s = \pm \frac{h_t}{2} \left( 1 - \frac{x_s^2}{(h_t a_t / 2)^2} \right)^n \quad (1)$$

Table 1 Geometric parameters for materials 1 (runs 1A-1Z) and 2 (runs 2A-2Z)

Run	Tow height (mm)	Tow width (mm)	In-plane spacing (mm)	Tow power (-)	Domain height (mm)	Domain in-plane size (mm×mm)	$v_{f,t}$ tow (-)	$v_{f,c}$ cell (-)
1A	1.0	6.0	1.0	0.3	1.10	26.0 × 26.0	0.829	0.611
1B	1.0	6.0	1.0	0.3	1.20	26.0 × 26.0	0.829	0.560
1C	1.0	6.0	1.0	0.5	1.10	26.0 × 26.0	0.872	0.611
1D	1.0	6.0	1.0	0.5	1.20	26.0 × 26.0	0.872	0.560
1E	1.0	4.0	1.0	0.3	1.10	18.0 × 18.0	0.861	0.611
1F	1.0	4.0	1.0	0.3	1.20	18.0 × 18.0	0.861	0.560
1G	1.0	4.0	1.0	0.5	1.10	18.0 × 18.0	0.906	0.611
1H	1.0	4.0	1.0	0.5	1.20	18.0 × 18.0	0.906	0.560
1Z	1.0	5.0	1.0	0.4	1.15	22.0 × 22.0	0.864	0.584

Runs 2A-2Z for balanced  $0/90^\circ$  material 2 have same parameters with doubled domain height.

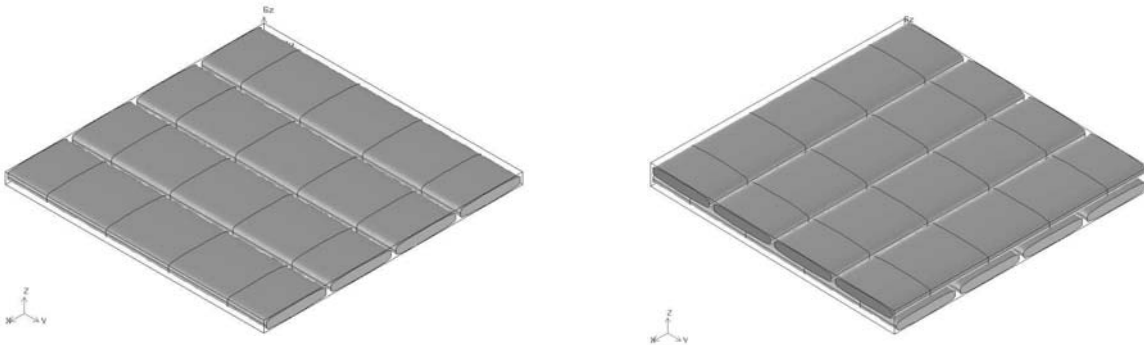


Fig. 1 Geometric models used in runs 1A (left) and 2A (right).

### IN-PLANE PERMEABILITY PREDICTIONS

In-plane flow simulations were conducted using Fluent™ 6.2.16. A mass flow rate of 0.1 g/s on the inlet face ( $x_{min}$  or  $y_{min}$ ) and null pressure on the outlet face ( $x_{max}$  or  $y_{max}$ ) were imposed. Other faces were set as walls. Tow permeabilities along ( $K_{||}$ ) and across ( $K_{\perp}$ ) fibres of radius  $r = 5 \mu\text{m}$  were calculated using Eqn. 2 [4] with  $v_{f,t}$  tabulated in Table 1. Darcy's law, Eqn. 3, was used for calculating cell permeability  $K_x$  or  $K_y$  along  $x$  and  $y$  from velocity  $u_x$  or  $u_y$  and average pressure gradient  $dP/dx$  or  $dP/dy$ . Resin viscosity  $\mu_r$  and density  $\rho_r$  were 0.1 Pa·s and 1.3 g/cm<sup>3</sup>. Resin flowed mostly outside of tows; resistance arose in narrow inter-tow gaps.

$$K_{||} = \frac{8r^2}{C} \cdot \frac{(1-v_{f,t})^3}{v_{f,t}^2}, \quad K_{\perp} = C_1 \left( \sqrt{\frac{v_{f,t,\max}}{v_{f,t}^2}} - 1 \right)^{5/2} r^2 \quad (2)$$

$$u_x = -\frac{K_x}{\mu_r} \cdot \frac{dP}{dx}, \quad u_y = -\frac{K_y}{\mu_r} \cdot \frac{dP}{dy} \quad (3)$$

Table 2 Results from flow simulations

Run		$K_{x,y}$ (m <sup>2</sup> )	Run		$K_{x,y}$ (m <sup>2</sup> )	Run		$K_{x,y}$ (m <sup>2</sup> )
1A	x	7.08×10 <sup>-11</sup>	1B	x	4.05×10 <sup>-10</sup>	1C	x	9.04×10 <sup>-11</sup>
	y	1.28×10 <sup>-9</sup>		y	1.67×10 <sup>-9</sup>		y	1.94×10 <sup>-9</sup>
1D	x	4.93×10 <sup>-10</sup>	1E	x	7.17×10 <sup>-11</sup>	1F	x	4.13×10 <sup>-10</sup>
	y	2.83×10 <sup>-9</sup>		y	1.51×10 <sup>-9</sup>		y	2.23×10 <sup>-9</sup>
1G	x	9.22×10 <sup>-11</sup>	1H	x	5.10×10 <sup>-10</sup>	1Z	x	1.00×10 <sup>-10</sup>
	y	2.21×10 <sup>-9</sup>		y	3.21×10 <sup>-9</sup>		y	2.10×10 <sup>-9</sup>
2A	x, y	2.05×10 <sup>-9</sup>	2B	x, y	4.29×10 <sup>-9</sup>	2C	x, y	3.23×10 <sup>-9</sup>
2D	x, y	5.97×10 <sup>-9</sup>	2E	x, y	2.27×10 <sup>-9</sup>	2F	x, y	4.49×10 <sup>-9</sup>
2G	x, y	3.40×10 <sup>-9</sup>	2H	x, y	6.12×10 <sup>-9</sup>	2Z	x, y	3.80×10 <sup>-9</sup>

### THROUGH-THICKNESS THERMAL CONDUCTIVITY PREDICTIONS

Through-thickness heat transfer simulations were conducted using Fluent™ version 6.2.16. A temperature difference of 5°C was imposed between walls  $z_{min}$  and  $z_{max}$ ; other walls were adiabatic. Tow conductivities ( $k_{||}$ ) and across ( $k_{\perp}$ ) fibres were obtained from Nielsen's model, Eqn. 4 [5]. Fourier's law, Eqn. 5, was used for calculating cell conductivity  $k_z$  along  $z$  from temperature gradient  $dT/dz$  and average heat flux  $q_z$ . Conductivity and specific heat of fibres and resin were 1.0 W/mK, 0.7 J/gK, 0.2 W/mK and 1.2 J/gK; fibre density was 1.75 g/cm<sup>3</sup>. The parameter having the strongest influence on  $k_z$  was the cell height, directly through its relation to

the thickness of resin-rich zones above and below tows and indirectly through its effect on  $v_{f,c}$ . Having two superimposed layers at 0/90° had little effect on  $k_z$ .

Table 3 Results from heat transfer simulations

Run		$k_z$ (W/mK)	Run		$k_z$ (W/mK)	Run		$k_z$ (W/mK)
1A	$z$	0.4822	1B	$z$	0.4363	1C	$z$	0.4766
1D	$z$	0.4327	1E	$z$	0.4859	1F	$z$	0.4388
1G	$z$	0.4813	1H	$z$	0.4357	1Z	$z$	0.4701
2A	$z$	0.4847	2B	$z$	0.4463	2C	$z$	0.4787
2D	$z$	0.4418	2E	$z$	0.4903	2F	$z$	0.4472
2G	$z$	0.4832	2H	$z$	0.4450	2Z	$z$	0.4612

$$k_{||} = k_f v_{f,t} + k_r (1 - v_{f,t}) \quad , \quad k_{\perp} = k_r \left[ \frac{1 + AB\phi}{1 - B\phi\phi} \right] \quad (4)$$

$$q_z = k_z \frac{dT}{dz} \quad (5)$$

### IN-PLANE STIFFNESS PREDICTIONS

In-plane static loading simulations were conducted using Abaqus™ 6.7-1. A tensile stress of 10 MPa was imposed along  $x$  or  $y$ . Displacements in other directions were not constrained but all faces had to stay flat. All other walls were free to move and remained flat. Tow stiffness along ( $E_{||}$ ) and across ( $E_{\perp}$ ) fibres were obtained from Eqn. 6 [6]. Eqn. 7 was used in calculating cell stiffness  $E_x$  or  $E_y$  along  $x$  and  $y$  from stress  $\sigma_x$  or  $\sigma_y$  and strain  $\varepsilon_x$  or  $\varepsilon_y$ . Fibre and resin stiffness  $E_f$  and  $E_r$  were 70 GPa and 5 GPa. Results were in line with expectations.

Table 4 Results from static loading simulations

Run		$E_{x,y}$ (GPa)	Run		$E_{x,y}$ (GPa)	Run		$E_{x,y}$ (GPa)
1A	$x$	15.64	1B	$x$	14.83	1C	$x$	16.87
	$y$	42.77		$y$	39.62		$y$	42.98
1D	$x$	16.01	1E	$x$	15.93	1F	$x$	15.13
	$y$	39.25		$y$	40.96		$y$	38.70
1G	$x$	17.14	1H	$x$	17.05	1Z	$x$	15.94
	$y$	40.72		$y$	37.44		$y$	40.11
2A	$x, y$	30.23	2B	$x, y$	28.30	2C	$x, y$	30.82
2D	$x, y$	28.82	2E	$x, y$	29.16	2F	$x, y$	28.17
2G	$x, y$	31.46	2H	$x, y$	28.56	2Z	$x, y$	29.17

$$E_{||} = E_f v_{f,t} + E_r (1 - v_{f,t}) \quad , \quad E_{\perp} = \frac{E_f E_r}{E_r v_{f,t} + E_f (1 - v_{f,t})} \quad (6)$$

$$E_x = \frac{\sigma_x}{\varepsilon_x} \quad , \quad E_y = \frac{\sigma_y}{\varepsilon_y} \quad , \quad \varepsilon_{x,y} = \frac{l - l_o}{l_o} \quad (7)$$

## DISCUSSION AND CONCLUSION

The fibre volume fraction of the cells varied between two set values, depending on cell height. These values were relatively close at  $v_{f,c} = 0.560$  and  $v_{f,c} = 0.611$ . Values of in-plane permeability varied strongly between the different cells, with two orders of magnitude separating lower and higher values. For unidirectional material 1 permeability was greater along the tows by one order of magnitude as observed with published experimental results. Permeability was smallest along  $x$  for thinner gaps above and below the tows, and it was largest along  $y$  when more numerous inter-tow channels encompassed tows of smaller section. The strongest parameter was direction, followed by cell height. Values for material 2 were larger than either value for material 1 because of the large gap along  $z$  between tows.

The transverse thermal conductivity was only marginally affected by reinforcement geometry with less than 15% separating minimum and maximum values for either reinforcement. It is notable that differences between unidirectional material 1 and bi-directional material 2 were negligible; this is explained by the large cover factor of each tow layer in material 2. It is also worth noting that whilst the larger inter-tow gap present at mid-thickness in material 2 has a strong effect on permeability it does not affect through-thickness conductivity. The parameter that most affects conductivity is the cell height, with in-plane tow spacing and section shape having comparatively marginal effects.

Values of in-plane stiffness generally behaved in accordance with the predictions of simple micromechanical models. Values of modulus for material 1 were larger along  $y$  and smaller along  $x$  with only small fluctuations resulting from changes in tow width or tow section shape. The effect of cell thickness simply resulted from the presence of thicker layers of resin-rich zones in the cell. Values of modulus along  $x$  or  $y$  observed for bi-directional material 2 corresponded roughly to averages of moduli along  $x$  and  $y$  for unidirectional material 1 with the same tow configuration, as predicted by the rule of mixture. This can be contrasted with permeability values for material 2 which were larger than either value obtained from material 1 in the same tow configuration.

The above results indicate that specific configurations will be preferable in view of different objectives. For example, thicker cells would be beneficial to the processing of a part made by VARTM but detrimental for composite tooling. One should consider the relative amplitude of changes in permeability, conductivity or stiffness when deciding on a configuration. Finally, the results show that accurate predictions of permeability require very precise geometric models whilst this is less critical with conductivity or stiffness.

## REFERENCES

1. C.C. Wong, A.C. Long, M. Sherburn, F. Robitaille, P. Harrison and C.D. Rudd, "Comparisons of Novel and Efficient Approaches for Permeability Prediction Based on the Fabric Architecture", *Composites Part A: Applied Science and Manufacturing*, Vol. 37, no 6 (SPEC. ISS.), 2006, pp. 847-857.
2. S. Hind, F. Robitaille and D. Raizenne, "Parametric Unit Cell Modelling of the Effective Transverse Thermal Conductivity of Carbon Plain Weave Composites", *Proc. 8<sup>th</sup> International Conference on Textile Composites (TEXCOMP-8)*, 2006.
3. J.J. Crookston, W. Ruijter, A.C. Long and I.A. Jones, "Modelling Mechanical Performance Including Damage Development for Textile Composites Using a Grid-Based Finite Element Method with Adaptive Mesh Refinement", *Proc. 8<sup>th</sup> International Conference on Textile Composites (TEXCOMP-8)*, 2006.
4. B.R. Gebart, "Permeability of Unidirectional Reinforcements for RTM", *Journal of Composite Materials*, Vol. 26, no. 8, 1992, pp. 1100-1133.
5. R. C. Progelfhof, J.L. Throne and R.R. Ruetsch, "Methods for Predicting the Thermal Conductivity of Composite Systems: a Review", *Polymer Engineering and Science*, Vol. 16, no. 9, 1976, pp. 615-625.
6. S.W. Tsai and H.T. Hahn, "Introduction to Composite Materials", *Technomic Publishing*, 1980, pp 377-428.